

# Cone Photoreceptor Abnormalities Correlate with Vision Loss in Patients with Stargardt Disease

Yingming Chen,<sup>1</sup> Kavitha Ratnam,<sup>2</sup> Sanna M. Sundquist,<sup>2</sup> Brandon Lujan,<sup>3</sup> Radha Ayyagari,<sup>4</sup> V. Harini Gudiseva,<sup>4</sup> Austin Roorda,<sup>3</sup> and Jacque L. Duncan<sup>2</sup>

**PURPOSE.** To study the relationship between macular cone structure, fundus autofluorescence (AF), and visual function in patients with Stargardt disease (STGD).

**METHODS.** High-resolution images of the macula were obtained with adaptive optics scanning laser ophthalmoscopy (AOSLO) and spectral domain optical coherence tomography in 12 patients with STGD and 27 age-matched healthy subjects. Measures of retinal structure and AF were correlated with visual function, including best-corrected visual acuity, color vision, kinetic and static perimetry, fundus-guided microperimetry, and full-field electroretinography. Mutation analysis of the *ABCA4* gene was completed in all patients.

**RESULTS.** Patients were 15 to 55 years old, and visual acuity ranged from 20/25–20/320. Central scotomas were present in all patients, although the fovea was spared in three patients. The earliest cone spacing abnormalities were observed in regions of homogeneous AF, normal visual function, and normal outer retinal structure. Outer retinal structure and AF were most normal near the optic disc. Longitudinal studies showed progressive increases in AF followed by reduced AF associated with losses of visual sensitivity, outer retinal layers, and cones. At least one disease-causing mutation in the *ABCA4* gene was identified in 11 of 12 patients studied; 1 of 12 patients showed no disease-causing *ABCA4* mutations.

**CONCLUSIONS.** AOSLO imaging demonstrated abnormal cone spacing in regions of abnormal fundus AF and reduced visual function. These findings provide support for a model of disease progression in which lipofuscin accumulation results in homo-

geneously increased AF with cone spacing abnormalities, followed by heterogeneously increased AF with cone loss, then reduced AF with cone and RPE cell death. (ClinicalTrials.gov number, NCT00254605.) (*Invest Ophthalmol Vis Sci.* 2011;52:3281–3292) DOI:10.1167/iov.10-6538

Stargardt disease/fundus flavimaculatus (STGD/FF) is characterized by autosomal recessive inheritance, reduced visual acuity, central vision loss, and characteristic yellow-white flecks at the level of the retinal pigment epithelium (RPE).<sup>1–4</sup> Histologic analyses show the accumulation of lipofuscin, a lipid-containing fluorophoric byproduct of photoreceptor digestion, within RPE cells.<sup>5–9</sup>

Disease-causing mutations in the *ABCA4* gene can be identified in up to 80% of patients with autosomal recessive STGD.<sup>10–17</sup> *ABCA4* encodes a photoreceptor-specific adenosine triphosphate-binding cassette transporter, ABCR, which is a phospholipid flippase found within the rims of rod and cone outer segments.<sup>10,15,18–20</sup> Abnormal ABCR leads to the intracellular accumulation of N-retinylidene-N-retinylethanolamine (A2E) in RPE cells.<sup>19,21,22</sup> A2E is the major fluorophore of lipofuscin, and its quantity in the fundus can be tracked by fundus autofluorescence (AF).<sup>23–27</sup> Fluorescein angiography of STGD/FF shows a characteristic “dark choroid” in which choroidal fluorescence is blocked by lipofuscin deposition within the RPE,<sup>2,28</sup> and AF shows abnormally high levels of lipofuscin in RPE cells.<sup>29</sup> Abnormalities in AF intensity, texture, and distribution have been characterized in patients with *ABCA4* mutations.<sup>11,12,23,27,29–34</sup>

Elevated levels of A2E within RPE cells may create a predisposition to apoptotic cell death through photo-oxidative damage<sup>35–37</sup> or toxic effects on normal RPE cellular processes.<sup>38–41</sup> Accumulation of A2E in RPE cells was hypothesized to be the earliest measurable abnormality in patients with *ABCA4* mutations, with subsequent death of the A2E-laden RPE cells and ultimately of the overlying photoreceptors.<sup>11</sup> However, the precise relationship between focally increased autofluorescence, focally decreased autofluorescence, and RPE atrophy is not monotonic,<sup>34</sup> and the exact mechanism of vision loss in patients with A2E accumulation, such as STGD, is not clearly understood.

Although several groups have reported on retinal structural changes in eyes with STGD/FF using spectral domain optical coherence tomography (SD-OCT),<sup>42–46</sup> it has been difficult to visualize the effects of A2E deposits on photoreceptors at the cellular level in living eyes because irregularities of the eye's optics limit the resolution of retinal images with all methods commonly used.<sup>47</sup> Adaptive optics can compensate for optical aberrations and improve the resolution of retinal images in normal eyes and in eyes with inherited retinal degenerations.<sup>48–60</sup> The present study sought to evaluate the relationship between AF abnormalities and vision loss using high-resolution imaging methods including SD-OCT and adaptive optics scanning laser ophthalmoscopy (AOSLO) in STGD pa-

From the <sup>1</sup>Faculty of Medicine, University of Toronto, Toronto, Ontario, Canada; <sup>2</sup>Department of Ophthalmology, University of California, San Francisco, San Francisco, California; <sup>3</sup>School of Optometry, University of California, Berkeley, Berkeley, California; and the <sup>4</sup>Department of Ophthalmology, University of California, San Diego, La Jolla, California.

Supported by a Career Development Award, a Physician Scientist Award, and an unrestricted grant from Research to Prevent Blindness (JLD); a Career Development Award and a Clinical Center Grant from the Foundation Fighting Blindness (JLD, AR); National Institutes of Health/National Eye Institute Grants EY002162 (JLD), EY014375 (AR), and K12 EY017269 (BJL); That Man May See, Inc. (JLD); The Bernard A. Newcomb Macular Degeneration Fund (JLD); Hope for Vision (JLD); the Karl Kirchgessner Foundation (JLD); and the National Science Foundation Science and Technology Center for Adaptive Optics, managed by the University of California at Santa Cruz under Cooperative Agreement AST-9876783 (AR).

Submitted for publication September 8, 2010; revised October 27 and November 23, 2010; accepted December 23, 2010.

Disclosure: **Y. Chen**, None; **K. Ratnam**, None; **S.M. Sundquist**, None; **B. Lujan**, Carl Zeiss Meditec, Inc. (C); **R. Ayyagari**, None; **V.H. Gudiseva**, None; **A. Roorda**, P; **J.L. Duncan**, None

Corresponding author: Jacque L. Duncan, Beckman Vision Center, UCSF School of Medicine, 10 Koret Way, Room K-129, San Francisco, CA 94143-0730; duncanj@vision.ucsf.edu.

tients. Clearer understanding of the relationship between AF abnormalities and retinal structure in living patients with disease-causing mutations in *ABCA4* may refine the models of pathogenesis in patients with STGD.

## METHODS

All studies adhered to the tenets of the Declaration of Helsinki. Informed consent was obtained from the subjects after explanation of the nature and possible consequences of the study. The experimental protocols were approved by the institutional review boards of the University of California at San Francisco and at Berkeley.

### Clinical Examination

Twelve subjects with STGD, ranging in age from 15 to 55 years, and 27 age-matched healthy subjects were studied. Each patient and healthy subject underwent a complete eye examination. Best-corrected visual acuity (BCVA) was measured using a standard eye chart according to the Early Treatment of Diabetic Retinopathy Study (ETDRS) protocol. Color vision was examined using the Farnsworth Dichotomous Test for Color Blindness (D-15; Psychological Corporation, New York, NY) followed by Lanthony's Desaturated D-15 Test (Richmond Products, Inc.; Albuquerque, NM) if there were no crossing errors on the Farnsworth panel. The data were analyzed using a Web-based platform scoring method (<http://www.torok.info/colorvision>), and the error scores were calculated using methods proposed by Bowman<sup>61</sup> and Lanthony<sup>62</sup> for the Farnsworth and Lanthony tests, respectively. Automated perimetry was performed with a visual field analyzer (Humphrey Visual Field Analyzer II; 750-6116-12.6; Carl Zeiss Meditec, Inc., Dublin, CA) 10-2 Swedish interactive threshold algorithm with measurement of foveal thresholds using a Goldmann III stimulus on a white background (31.5 asb) and exposure duration of 200 ms. Goldmann kinetic perimetry was performed using V-4e and I-4e targets. Pupils were dilated with 1% tropicamide and 2.5% phenylephrine. Color fundus photographs and fluorescein angiography studies were acquired using a digital fundus camera (50 EX; Topcon, Livermore, CA). AF images were taken using either a digital fundus camera equipped with AF filters (Ophthalmic Imaging Systems, Inc., Sacramento, CA), similar to a system previously described,<sup>63</sup> or a scanning laser ophthalmoscope system (Spectralis 3.1 HRA+OCT; Heidelberg Engineering, Vista, CA) using a 488-nm light source for excitation after reducing the power at the camera and using the 95% sensitivity setting, as previously described.<sup>23</sup> SD-OCT images were obtained with the same scanning laser ophthalmoscope system used to acquire some AF images as described above (Spectralis 3.1 HRA+OCT; Heidelberg Engineering) using the infrared beam of the superluminescent diode (central wavelength, 870 nm). Scans averaged 100 A-scans/B-scans for 30° horizontal and vertical images through the locus of fixation, and 10 A-scans/B-scans for the 19 horizontal scans used to acquire the 20° × 15° volume scans. In the figures, all scans through fixation are 100-frame line B-scans, whereas scans located eccentric to fixation (such as over focal autofluorescence abnormalities or flecks) are 10-frame B-scans from the volume scan. In the figures, all scans through fixation are 100-frame line scans, whereas scans located eccentric to fixation (such as over focal autofluorescence abnormalities or flecks) are 10-frame scans from the volume scan. Fundus-guided microperimetry (MP-1; Nidek Technologies America Inc., Greensboro, NC) tested 45 locations within the central 8° visual field, as previously described,<sup>57-59</sup> using a white Goldmann III stimulus of 200-ms duration with a 4-2-1 threshold strategy on a white background. Stability of fixation at the preferred retinal locus (PRL) was evaluated by asking subjects to focus on the center of four 2° crosses located 5° eccentric to fixation. Numeric microperimetry results were superimposed onto AF and AOSLO images after image scaling and registration using image editing (Photoshop; Adobe, Mountain View, CA) and custom-written (MatLab; The MathWorks, Natick, MA) software. Mean ± 1 SD normal values across the central 10° were as follows: for subjects aged 20, 19.9 ± 0.4 dB; for subjects aged 21 to

40, 19.5 ± 1.1 dB; for subjects aged 41 to 60, 19.3 ± 1.3 dB (Midena et al., *IOVS* 2006;47:ARVO E-Abstract 5349). Full-field electroretinography (ERG) was performed after 45 minutes of dark adaptation using a Burian-Allen contact lens electrode (Hansen Ophthalmic Development Laboratory, Iowa City, IA), according to International Society for Clinical Electrophysiology and Vision standards, as previously described.<sup>57-59,64</sup>

### Genetic Testing

Whole blood was obtained from each patient, and genotyping was carried out through the National Ophthalmic Disease Genotyping Network (eyeGENE; National Eye Institute, Bethesda, MD; University of Michigan Ophthalmic Molecular Diagnostic Laboratory, Ann Arbor, MI; University of California, San Diego, San Diego, CA; Columbia University Medical Center, New York, NY; and GeneDX, Gaithersburg, MD). Mutation analysis of the *ABCA4* gene was carried out by sequencing the complete coding region in 10 of the 12 patients using dideoxy sequencing. Mutation analysis of two additional patients was carried out by sequencing the coding region on the Illumina (San Diego, CA) platform, and the sequence changes detected were confirmed by dideoxy sequencing (Smaoui N, GeneDX, personal communication, 2010).

### AOSLO Imaging and Image Processing

AOSLO images were obtained<sup>57-59</sup> and processed to create montages from all patients and from 27 age-matched healthy subjects. Quantitative cone spacing measures were performed on images from 8 of the 12 patients in whom unambiguous cone mosaics were observed; quantitative cone spacing measures were not possible in 4 of the 12 patients (F6P1, F8P1, F9P1, and F10P1) because of the lack of unambiguous cone mosaics in the montage, as a result of unstable fixation and/or cone atrophy in areas of reduced vision. Images of all 12 patients are shown in Supplementary Figures S1 to S13 (<http://www.iovs.org/lookup/suppl/doi:10.1167/iovs.10-6538/-/DCSupplemental>). Supplementary Figure S1 shows AF, SD-OCT, and AOSLO montages acquired surrounding each subject's preferred locus of fixation. Supplementary Figures S2 to S13 show large, high-resolution AOSLO images for each patient. The eye with better visual acuity or more stable fixation was chosen for imaging studies. The preferred locus of fixation was determined by having the subject fixate on a blinking black circle that was modulated within the laser raster. Because the laser that formed the image was used to modulate the fixation spot, the fixation locus was encoded onto the recorded video and determined with micrometer accuracy. Additional videos were recorded in the parapapillary regions.

### Cone Spacing Analysis

Scales of the macular images were calculated using a calibrated standard grid captured before each imaging session. Regions of the image in which a contiguous cone mosaic, identified as regions containing a close-packed arrangement of reflective spots, was clearly visualized were selected for spacing measurements. The presence of cones in each region was further established by the visualization of the inner segment-outer segment (IS/OS) junction in registered SD-OCT scans. Individual cones within the mosaic were identified manually, and the average nearest-neighbor spacing was determined using the first peak in the density recovery profile.<sup>51,65</sup> Cone spacing was chosen over cone density as a measure of photoreceptor distribution because it provided the most robust and conservative assessment for comparison among eyes. Cone spacing measures quantify average cone spacing in selected regions only and cannot be extrapolated to predict spacing in surrounding regions. In diseased eyes, particularly of the types in this study, there were many regions within each AOSLO image in which no unambiguous cone mosaics were resolved. Cone spacing, therefore, should be considered only one aspect of image analysis.

## Statistical Analysis

To compare the difference in cone spacing between the eyes of patients with STGD and normal eyes, spacing measurements of all subjects were plotted against their corresponding locations on the retina. Locations of parafoveal cones were measured as eccentricity in degrees relative to the anatomic fovea, whereas locations of parapapillary cones were measured as eccentricity in degrees relative to the optic nerve head (ONH) to account for interindividual differences in the foveo-papillary distance. Distance to the ONH was defined as the perpendicular distance between the cone mosaic and the tangent of the scleral rim. Cone spacing for STGD patients was compared with the mean from 27 age-matched healthy subjects, as previously described.<sup>57-59</sup> Least-squares fit was used to generate a curve predicting the mean normal cone spacing with 95% confidence intervals at each eccentricity. Cone spacing data were quantified using z-scores, the number of standard deviations from the mean at the eccentricity measured. Measurements within  $\pm 2$  SD, or z-scores between  $-2$  and  $+2$ , were considered normal.  $P < 0.05$  was considered statistically significant.

## RESULTS

STGD patients ranged in age from 15 to 55 years. Visual acuity ranged from 20/25 to 20/320. Full-field ERG amplitudes and implicit times were normal for all stimuli tested for all patients. Healthy subjects ranged in age from 14 to 72 years, and their BCVA was between 20/15 and 20/20.

Mutation analysis of the *ABCA4* gene identified at least two heterozygous mutations in seven patients, including two siblings from a pedigree, one mutation in four patients, and no mutations in one patient. Although the presence of two or more mutations in the *ABCA4* gene is necessary to cause STGD, approximately 25% of patients with a diagnosis of STGD are reported to carry one or no mutations in this gene.<sup>17</sup> We did not observe correlations between phenotype and genotype. Findings from clinical examinations and genetic analysis for patients are summarized in Table 1.

### Abnormal Autofluorescence, SD-OCT, and AOSLO in Patients with STGD

AOSLO imaging revealed regions of abnormal cone structure in the maculae of all patients with varying degrees of abnormality, described here in order of increasing severity. In several patients with advanced macular atrophy, unstable fixation resulted in AOSLO image quality that was not adequate to permit quantitative cone spacing measures (Supplementary Fig. S1, <http://www.iovs.org/lookup/suppl/doi:10.1167/iovs.10-6538/-/DCSupplemental>).

### Cone Structure in Areas of Homogeneous Autofluorescence without Clinical Flecks

The least severe structural abnormalities were observed in regions of homogeneous AF without clinically evident flecks or RPE abnormalities, in which AOSLO images revealed contiguous cone mosaics of normal or near-normal spacing where unambiguous cones were visualized (Figs. 1B1-1B3). In regions of homogeneous AF, cone spacing values often fell within normal limits (z-scores  $\leq \pm 2$ ). However, cones were sparse and not regularly arranged at the fixation locus (Fig. 1B4). Finally, in regions of RPE atrophy at the anatomic fovea, unambiguous cones were not reliably seen (Fig. 1B5), corresponding to loss of the IS/OS junction on SD-OCT (Fig. 1C).

### Cone Structure in Patients with Central Fixation and Heterogeneous Autofluorescence

Based on anatomic landmarks from the SD-OCT images, including the base of the foveal pit and the center of the region at the

fovea lacking inner retinal neurons, we concluded that fixation was at or near the anatomic fovea in three patients (F1P1, F2P1, F11P1) in whom AF was heterogeneous and irregular (Figs. 2A, 2D, 2G). F1P1 showed an island of coarse, hyperreflective cones at the anatomic fovea surrounded by a hyporeflexive annulus with a radius from 0.25 to approximately  $1^\circ$  in which cones were not clearly visualized (Fig. 2B1). Cones were irregularly packed. In selected regions within the central  $4^\circ$  where we could identify contiguous mosaics, cone spacing was variable, showing regions with normal, reduced, and increased cone spacing (z-scores =  $-2.47$ – $4.60$ ). Sensitivity loss was patchy, with values ranging from 1 to 18 dB; foveal sensitivity was reduced by 1 log unit (10 dB) (Fig. 2B). Foveal cones in F2P1 were also hyperreflective and disorganized, with increased spacing at fixation (z-score = 4.38). Across most of the image, hyperreflective spots, suggestive of cones, were visible, but few close-packed mosaics could be identified. Where mosaics were identified, we found a mix of normal and increased cone spacing (Fig. 2E1). Sensitivity was well preserved and normal (20 dB) at most locations despite the patchy cone mosaic, but it was reduced by almost 2 log units (2 dB) in a hyporeflexive region temporally, where unambiguous cones could not be visualized. SD-OCT images at the foveas of both F1P1 and F2P1 showed disruption of the IS/OS junction, loss of the outer nuclear layer, and decreased foveal thickness (Figs. 2C, 2F).

Foveal structure was preserved in an island surrounded by RPE atrophy in F11P1 (Figs. 2G, 2H). Cone spacing was increased near the fovea (z-scores = 3.91–8.44), and sensitivities were reduced by greater than 1.5 log units despite visual acuity of 20/25. The SD-OCT image of F11P1 showed preserved retinal and RPE structures at the fovea; however, the RPE was thickened and associated with shadows posteriorly, and the IS/OS junction was attenuated (Fig. 2I). In each patient with central fixation, foveal cones were coarse and hyperreflective. In F1P1, foveal fixation was retained even when greater sensitivity values were measured eccentric to the fovea (Fig. 2B).

Although all three patients retained foveal fixation, we found that F1P1 and F2P2 adopted an eccentric fixation locus for some tasks. F1P1 used the anatomic fovea to fixate a blinking black target that was modulated within the 840-nm scanning raster but resorted to an eccentric location to fixate the 532-nm fixation light. Conversely, F2P1 used an eccentric location to fixate a dim blinking spot within the raster but used the anatomic fovea to track the 532-nm fixation light.

### Relationship between Cone Structure and Clinical Flecks

Flecks characteristic of STGD were observed in some patients in transitional regions between centrally reduced AF, representing RPE atrophy, and homogeneous AF at greater eccentricities. Focal hyperautofluorescent regions correlated with yellow flecks were associated with subretinal hyperreflective deposits on SD-OCT (Figs. 3E-E2). AOSLO images showed highly reflective structures over the flecks (Fig. 3E1). SD-OCT scans through focal hyperautofluorescent flecks revealed dome-shaped deposits in or on the RPE layer (Fig. 3E2). The deposits disrupted the layer of the IS/OS junction, with larger deposits elevating or penetrating the external limiting membrane (ELM). The IS/OS junction was absent in both images, correlating with the lack of visible cone mosaics in this region (Fig. 3E). Both hyperautofluorescent and hypoautofluorescent flecks were observed in association with highly reflective structures on AOSLO (Figs. 3G, 3H), which most likely did not represent wave-guiding cones because they were not arranged in a contiguous mosaic and were not associated with an intact IS/OS junction on the corresponding SD-OCT images.

TABLE 1. Clinical Characteristics of the Patients with Stargardt Disease

Patient/Eye	Age (y)/Sex	ABC44 Mutations	BCVA	ETDRS Score	Color Vision*	Goldmann Visual Field†	Humphrey Visual Field 10–2	Foveal Threshold (dB)	Fixation
F1P1 OS	16/M	Pro1486 Leu/6 bp ins + 32 bp del at base 672	20/40	75	None, 0, 1.34	V4e: full; 14e: 1° ctl scotoma	8° ctl scotoma with <1° log unit sensitivity loss	30	Foveal
F1P2 OS	15/M	Pro1486 Leu/6 bp ins + 32 bp del at base 672	20/160	40	NS, 2, 1.99	V4e: full; 14e: 1° ctl scotoma	Dense scotoma beginning 4° superior to fixation	27	Superior
F2P1 OS	25/F	Glu1412stop	20/63	61	None, 0, 1.00	V4e, 14e: full, 12e: 5° ctl scotoma	6° ctl scotoma	31	Foveal
F3P1 OD	24/M	Gly863Ala	20/100	50	NS, 6, 2.72	V4e: full; 14e: 3–4° ctl scotoma	3°–4° scotoma superior to fixation	32	Superior
F4P1 OS	16/F	No disease-causing mutations identified	20/200	35	NS, 5, 2.25	V4e: full; 14e: 35° ctl scotoma	15° ctl scotoma with eccentric fixation superonasally	8	Nasal, slightly below horizontal meridian
F5P1 OS	42/M	5461-10 T>C intron 39/Gly1961Glu	20/320	23	NS, 5, 2.27	V4e: full; 14e: 10° ctl scotoma	12° dense ctl scotoma	27	Superonasal
F6P1 OS	19/F	Lys 223 Gln/C 2291 15 bp/5 amino acid deletion (CSGVI)	20/200	35	NS, 6, 1.99	V4e: full; 14e: 35° ctl scotoma	10° ctl scotoma	20	Superonasal
F7P1 OS	55/F	Arg212Cys/Gly863Ala/Thr959Ile	20/160	40	NS, 3, 2.01	V4e: 10° ctl scotoma; 14e: 20° ctl scotoma	Dense 15° ctl scotoma	6	Superonasal
F8P1 OS	36/M	Ser336Cys/Arg1068/Ser ‡	20/200	34	NS, 8, 3.62	V4e: 20° ctl scotoma; 14e: 25° ctl scotoma	Dense scotoma beginning 6° superior to fixation	12	Superior
F9P1 OS	28/M	Arg1108His/Val1433Ile	20/320	25	NS, 11, 3.30	V4e: full; 14e: 15° scotoma from 5–25° superior to fixation	Dense scotoma beginning 5° superior to fixation	23	Superior
F10P1 OS	55/F	IVS20 + 5 G > A splice/Gly1961Glu	20/320	25	NS, 6, 2.55	V4e: 30° ctl scotoma; 14e: 35° ctl scotoma	Dense scotoma extending from fixation to 10° inferonasally	19	Inferonasal
F11P1 OS	50/M	Arg2030Gln	20/25	80	Tritan, 7, 2.61	V4e: full; 14e: 25° ctl scotoma from 10–25° with foveal sparing	Dense scotoma extending from fixation to 10° with foveal sparing	27	Foveal

ctl, central; F, family; F, female; M, male; NS, nonspecific orientation; OD, right eye; OS, left eye; P, proband.

\*Lanthony's Desaturated Test results are shown for all patients except F9P1, F10P1, and F11P1, for whom the Farnsworth D15 results are shown. All other patients made no errors on the Farnsworth D15 test. Farnsworth D15; orientation, number of diametrical crossings (d.c.), and Color Confusion Index (CCI) based on Bowman scoring method; normal = 1.00.<sup>61</sup> Lanthony's Desaturated D15; orientation, d.c. and CCI based on Lanthony scoring method.<sup>62</sup>

† Greatest diameters of scotomas are reported, measured in degrees.

‡ This variant is not in a structural motif but is near the adenosine triphosphate-binding domain signature motif C and is predicted to be damaging.

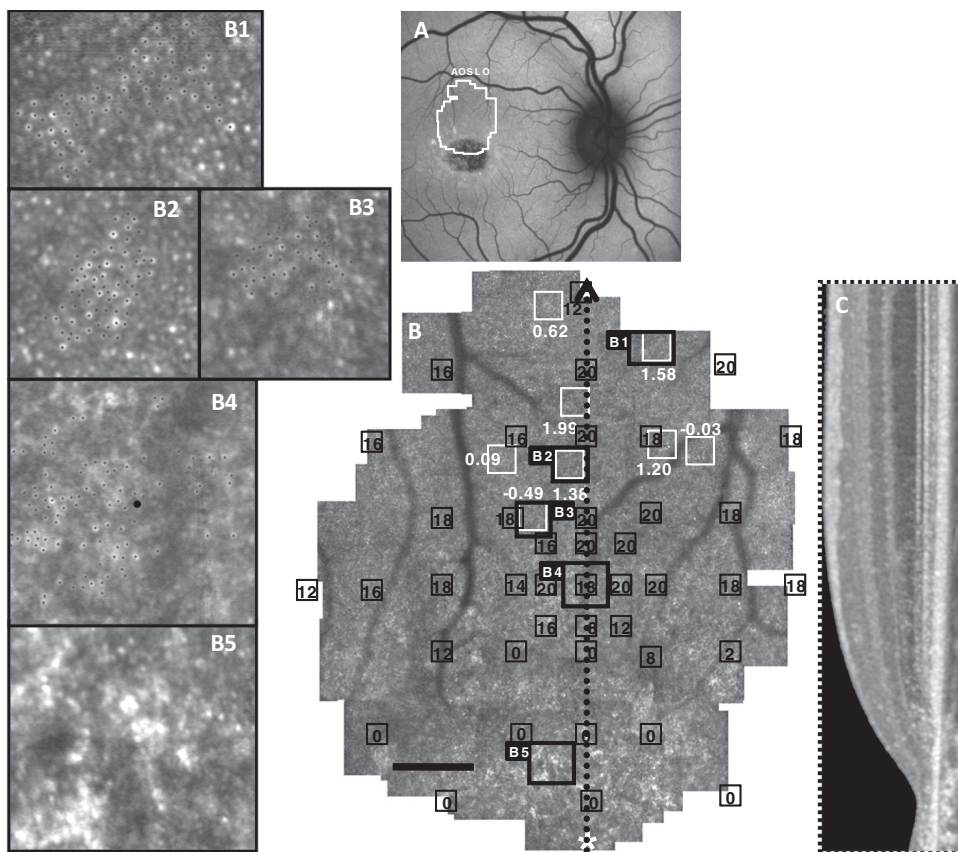


**FIGURE 1.** Images of F3P1: (A) AF. (B) AOSLO with MP1 sensitivities (black boxes and values, dB) and cone spacing measurements (white boxes and values, z-scores). (C) Vertical SD-OCT transecting fixation. (B1-B3, insets) Cones used for cone spacing measures (black dots). (B4) PRL with abnormal cone morphology. (B5) Lack of unambiguous cones in a region of RPE atrophy surrounding the anatomic fovea (\*). Scale bar, 1°.

**Lack of Unambiguous Cones in Transitional Regions between Atrophy and More Normal Outer Retinal Structure**

The transition zone between centrally reduced AF and homogeneous AF at greater eccentricities showed dim reflectance

containing sparse cones with increased cone spacing in AOSLO images (Fig. 3D, between black dashed lines). In patient F1P1, a dim region with sparse cones was observed within the region of heterogeneous AF; cone contiguity and packing regularity increased with increased distance from the fovea and proxim-

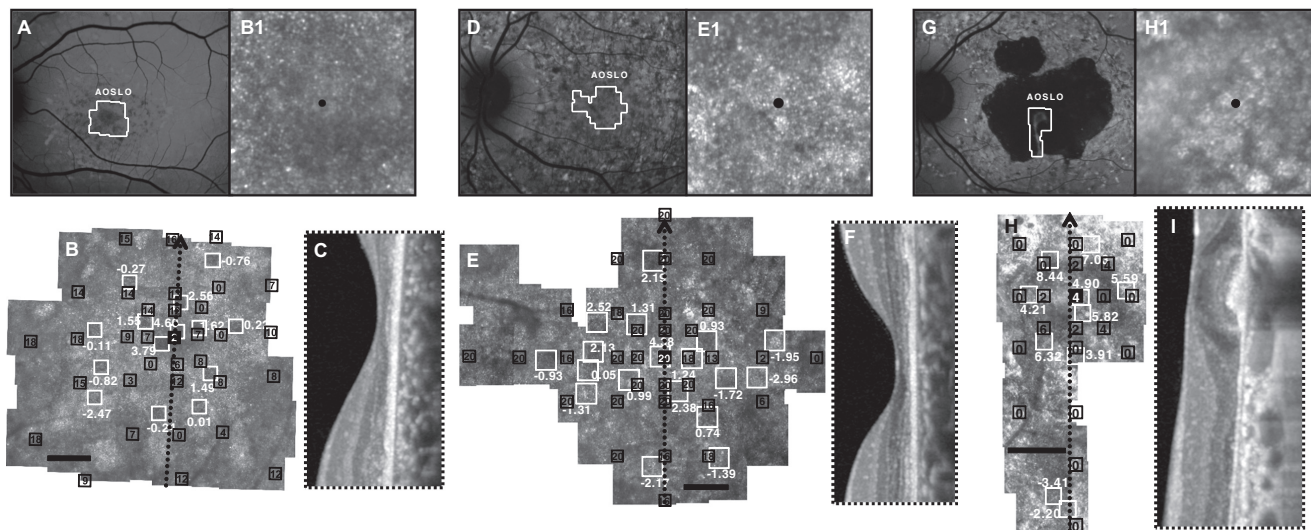


**FIGURE 2.** Cone structure in Stargardt patients with foveal sparing. Images of F1P1: (A) AF. (B) AOSLO with MP1 sensitivities and cone spacing. (B1, inset) Dim cones at the anatomic fovea (black dot). (C) SD-OCT shows disrupted IS/OS junction at the fovea. Images of F2P1: (D) AF. (E) AOSLO with MP1 sensitivities and cone spacing. Cone spacing was patchy with variable spacing relative to normal. (E1, inset) Coarse cones at the fixation locus, the anatomic fovea (black dot). (F) SD-OCT shows disrupted IS/OS junction at the fovea. Images of F11P1: (G) Fundus autofluorescence; (H) Cone spacing was significantly increased where sensitivities were measurable near the anatomic fovea (H1, inset, black dot). (I) SD-OCT shows preserved retinal and RPE structure at the fovea, although the RPE is thickened and associated with shadowing posteriorly, and the IS/OS junction is attenuated. For all three subjects, MP1 sensitivities (black boxes and values, dB) and AOSLO cone spacing measurements (white boxes and values, z-scores) are superimposed. Black scale bar, 1° (B, E, H).

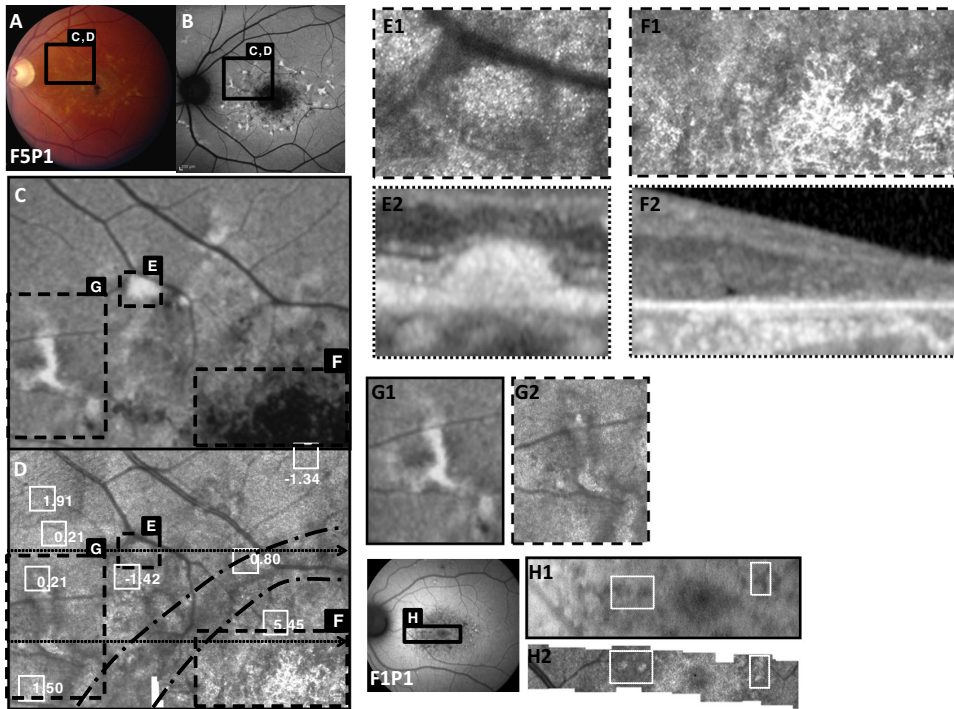


**FIGURE 3.** Images of F5P1 (A–G) and F1P1 (H): (A) Fundus. (B) AF. (C) Enlarged AF image of the region outlined in black in (A) and (B). (D) Corresponding AOSLO image with cone spacing measurements at locations outlined with *white square boxes* indicated with z-scores, or numbers of standard deviations away from the normal mean at that location. (E, F) Enlarged AOSLO (E1, F1) and SD-OCT (E2, F2) images of the regions outlined with *dashed lines* in (C) and (D). (D, dotted arrows) Positions of SD-OCT scans. Hyperreflective structures are present over flecks (E1, E2). (D) Area between *black dashed lines* indicates the transition zone between intact and absent cones. Hyperreflective regions without cones (F1) are seen in regions of atrophy on AF (F) and SD-OCT (F2). (G, H) Hyperreflective structures seen on AOSLO (G2, H2) correlate to both hypoautofluorescent regions on AF (G1) and in other patients hyperreflective structures correlate to hyperautofluorescent regions on AF. (H1) Patient F1P1.

ity to the optic nerve (Fig. 4A). Horizontal SD-OCT scans across the region showed a transition from preserved retinal layers to outer retinal layer disruption, then complete loss of the IS/OS junction layer correlating with the transition to sparse, and then absent, cones (Fig. 4B). Similar transition zones of hyporeflectivity and absence of cones were found in AOSLO images of F5P1 (Fig. 3D) and F7P1 (not shown). The transition zone showed interme-

diated sensitivity corresponding to the lack of outer retinal layers on SD-OCT and lack of cones on AOSLO (Fig. 4A3).

**Lack of Cones Where OCT IS/OS Layers Are Missing**

Regions of hypoautofluorescence corresponded to bright areas on AOSLO in which unambiguous cones were not visualized

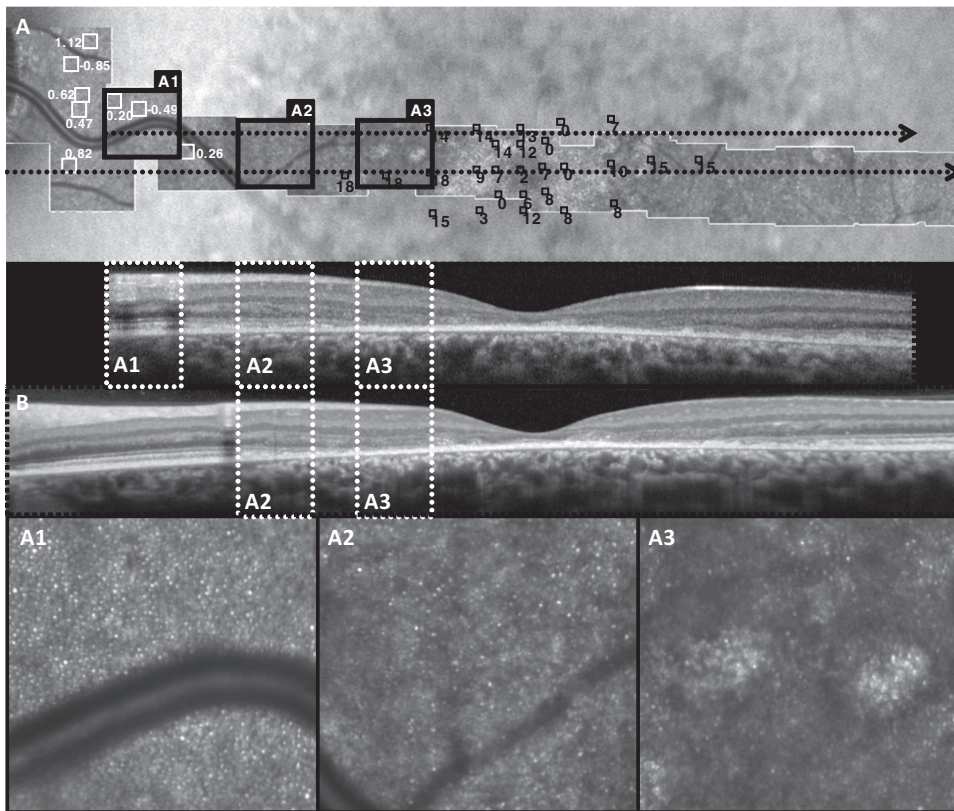


**FIGURE 4.** Dim regions with sparse cones are found in the transition zone between atrophy and more normal outer retinal structure. (A) AOSLO image with MP1 overlay and cone spacing measurements at locations outlined with *black and white square boxes*, respectively, in patient F1P1. *Insets* in the lower panel are outlined with *bold squares* on the AOSLO montage. (B) Two horizontal SD-OCT scans, the lower scan transecting the fovea, are shown, with regions corresponding to the same *insets* outlined with *white dashes*. Cone spacing measures were normal where cones were visualized near the disc (A1), whereas sparse cones were seen in transitional regions with preserved sensitivity (*small black square boxes*). The IS/OS junction was visible on SD-OCT (B) in regions with normal cone spacing (A1) and between normal cones and atrophy (A2), but unambiguous cones were not seen where the IS/OS junction was disrupted (A3).

and SD-OCT showed outer retinal atrophy (Figs. 3F1, 3F2). Figure 3F1 shows the AOSLO image of a region of atrophy in the left eye of F5P1, revealing bright, oversaturated areas devoid of cones, likely caused by scattering of infrared light from pigment. SD-OCT scans showed extensive loss of outer retinal layers, from the IS/OS junction to the inner nuclear layer, in regions of central RPE atrophy and reduced AF (Fig. 3F2).

### Preserved Cone Structure at Preferred Retinal Loci

Fixation was extrafoveal in nine patients with central atrophy; seven patients had superior or superonasal fixation, and two had inferonasal fixation. On SD-OCT, the retinal locus of extrafoveal fixation was located in a transition zone in which the outer nuclear layer and the inner and outer segment layers were present but thin and disrupted (Fig. 5). Although retinal layers and cone spacing often appeared more normal distal to the locus of fixation, fixation was located at a region closest to the anatomic fovea with preserved cone mosaics despite compromised cone spacing (as in Fig. 1B).

### Parapapillary Cone Spacing in Patients with STGD

AOSLO images of patients with STGD showed cone spacing and packing that was best preserved and most similar to normal near the ONH (Figs. 6A, 6B). Figure 6C shows cone spacing approaching normal beyond 5° from the fovea in all patients. Cone spacing fell within the normal range in the parapapillary region in all patients (Fig. 6D). AF was most homogeneous in an annulus at least 0.6 mm wide,<sup>12</sup> extending temporally from the ONH edge in all patients, even those with heterogeneous AF beyond the ONH (F2P1, F4P1). In all patients the IS/OS junction was most normal adjacent to the ONH (example shown in Supplementary Fig. S1 [http://www.iovs.org/lookup/suppl/doi:10.1167/iovs.10-6538/-/DCSupplemental], patient F4P1).

### Intervisit Progression

We studied two patients longitudinally using AOSLO, AF, and SD-OCT (F1P1 and F2P1; Fig. 7). During three visits over 27 months, the region of heterogeneous AF adjacent to the central region of reduced AF extended in all directions in F1P1. Increased hypoautofluorescent and hyperautofluorescent spots were observed, with reduced AF centrally and increased AF at greater eccentricities. Because of a problem with detector saturation, we were unable to make reliable cone spacing measurements on the images obtained in the first visit. Between the second and third visits (12.5 months apart), AOSLO images of F1P1 showed no systematic changes in cone spacing in retinal regions common to both visits where unambiguous cone mosaics were identified. However, over the course of the three visits, there was an apparent loss of the foveal cones, with concurrent reduction in visual acuity from 20/40 (ETDRS score = 75) to 20/50 (ETDRS score = 68) and decreased central visual sensitivity on microperimetry (Figs. 7A1-2, 7B1-2). The AOSLO image at fixation from the third visit, 27 months after the first, revealed scattered regions in which polygonal

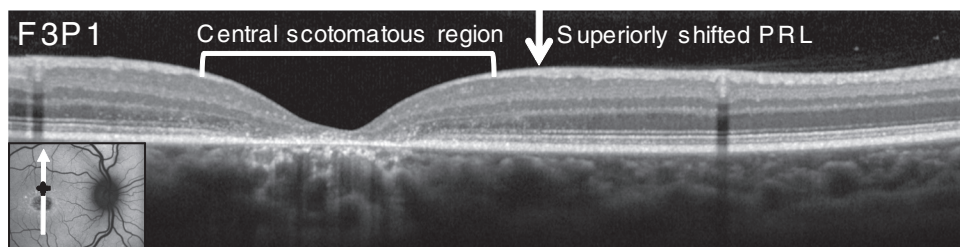
structures characteristic of RPE cells<sup>57</sup> were present between sparse foveal cones (Fig. 7C1, arrows). This was accompanied by further reduction of the central visual sensitivity, although visual acuity remained stable at 20/50 (ETDRS score = 67; Fig. 7C2). At the third imaging session, patient F1P1 used the anatomic fovea when asked to look at a small, dim, blinking target but used an eccentric retinal location approximately 3° nasal to the anatomic fovea to view the larger, bright, steady fixation target (Fig. 7C1). Although cone photoreceptors did not appear as a complete and contiguous mosaic anywhere in this patient, the cones were more readily visible at the new PRL than at the anatomic fovea, and, where cones could be measured, their spacing was within normal limits for that eccentricity. This shift in the PRL explains the poor overlap of the AOSLO montage from the latest visit compared with the first two and limited our ability to make more extensive comparisons of cone spacing between sessions.

F2P1 was examined twice in 27 months. AF images from the two visits appeared similar, though the number of hyperautofluorescent spots increased in the posterior pole in the more recent image (Figs. 7D, 7E). AOSLO images showed coarse, disorganized cones at the fovea at both visits, with preserved visual sensitivity at the fovea but decreased sensitivity at several locations (Figs. 7D1-2, 7E1-2). Visual acuity was stable, if not improved, during this interval; acuity measured 20/63 (ETDRS score = 61) at the first visit and 20/50-2 (ETDRS score = 63). However, microperimetry showed reduced sensitivity at a number of locations near the fovea at the second visit (Fig. 7E2) compared with the first (Fig. 7D2). Cone spacing was increased in some regions throughout the central macula, though many regions had cone spacing that fell within normal limits. The patient used the anatomic fovea to fixate the 532-nm fixation light but used an eccentric location to fixate the dim red blinking spot modulated within the 840-nm raster. The PRL location was in a similar direction for both visits (2.5° nasal), but, at the second visit, the mean location had shifted down by approximately 1°.

### DISCUSSION

STGD is associated with an accumulation of lipofuscin within RPE cells, which contains A2E, a fluorophore shown to be toxic to RPE cells.<sup>35,36,39,66,67</sup> We used AOSLO, SD-OCT, AF, and fundus-guided microperimetry to study macular cone structure, lipofuscin deposition, and visual function in patients with STGD and investigated longitudinal progression in two patients over 27 months. In 4 of 12 patients, disease severity resulted in unstable fixation and extensive cone loss in the macula, which precluded the acquisition of AOSLO images of cones that were of sufficient quality to perform quantitative cone spacing measures. AOSLO may be less useful than AF and SD-OCT for evaluating retinal structure in patients with advanced macular atrophy. However, in the remaining eight patients, our results showed abnormal AF in association with abnormalities of cone morphology and packing structure, suggesting a correlation between increased AF and loss of photoreceptor cells.

**FIGURE 5.** SD-OCT scan through the anatomic fovea (white arrow in inset AF image) and PRL of fixation (black plus sign in inset) of patient F3P1 with eccentric fixation and central atrophy. The region of eccentric fixation was located in a transition zone where the outer nuclear layer and the IS and OS layers were present but were thin and disrupted.



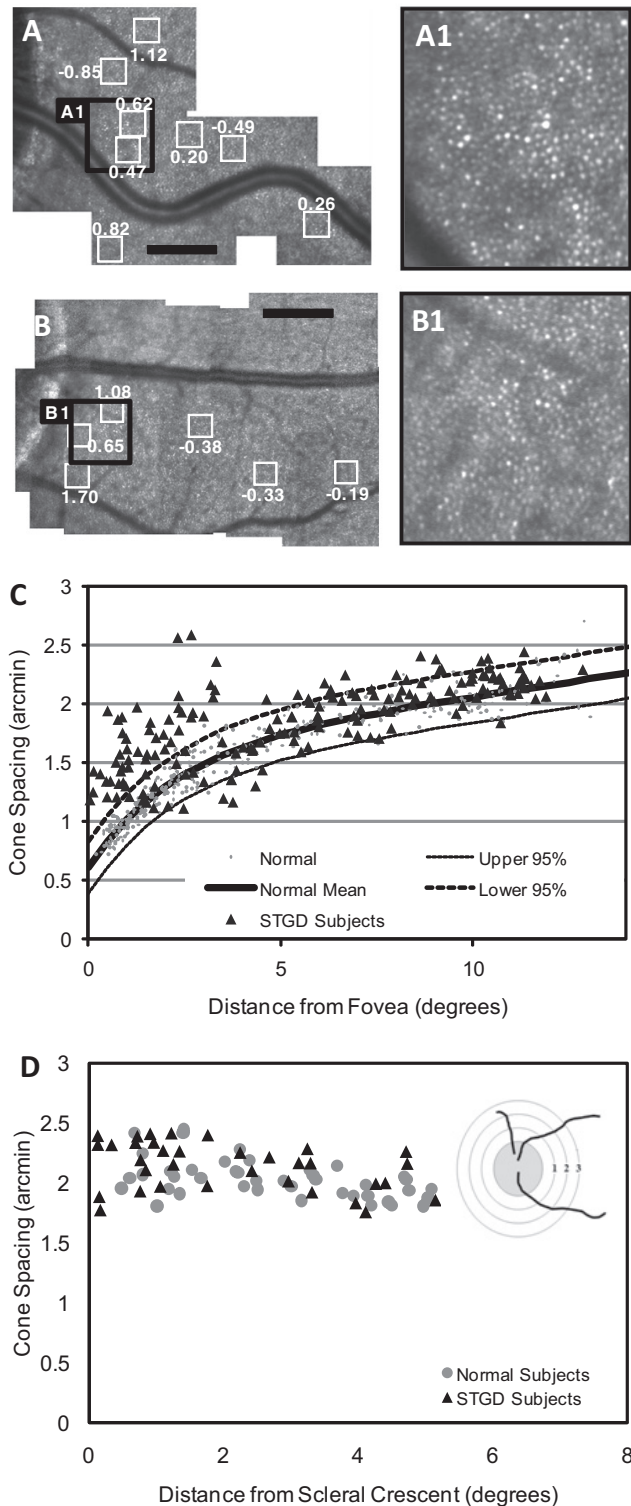


**FIGURE 6.** Normal cone spacing near the optic disc. AOSLO images in the parapapillary region of F1P1 (**A**) and a healthy subject (**B**). Cone spacing measurements in various locations (*white boxes* around the ONH) are shown. Black scale bar, 1°. (**A1**) and (**B1**) are magnified images of the regions shown on the larger montages (**A**) and (**B**). (**C**) Cone spacing versus distance from the fovea. Cone spacing measurements on AOSLO were obtained for 8 of 12 patients in the study. Measurements were not performed for 4 of 12 patients (F6P1, F8P1, F9P1, F10P1) because of the lack of unambiguous cone mosaics in the imaged region as a result of unstable fixation or cone atrophy in areas of reduced vision. (**D**) Cone spacing versus distance from the scleral

Consistent with previous studies,<sup>14,31,68–71</sup> the present study demonstrated abnormal AF in the macula of all STGD patients. AF can be used to track lipofuscin accumulation and provides an indirect way of assessing the overall health of RPE cells over a large area,<sup>72,73</sup> but the relatively low resolution of this imaging modality precludes the investigation of individual cellular structures. We have correlated high-resolution images of cone photoreceptor structure with AF and observed abnormalities of cone structure in order of increasing severity.

We observed normal or near-normal cone spacing, cross-sectional retinal structure, and visual sensitivity in regions of homogeneous AF. For example, F3P1 showed homogeneous AF without clinical flecks outside the fovea, corresponding to near-normal cone spacing. Closer to the fovea, cone spacing was increased in an area with focal increased AF near the central region of atrophy (Fig. 1). Flecks on examination and AF provided signs of clinical disease, with the flecks corresponding to dome-shaped deposits in the RPE layer seen on SD-OCT. Deposits elevated and disrupted the IS/OS junction and ELM layers (Fig. 3E). Hyperreflective regions seen on AOSLO images were observed with both hyperautofluorescent and hypoautofluorescent regions (Figs. 3G, 3H), demonstrating that AOSLO image reflectivity does not correlate with the quantity of lipofuscin accumulation in RPE cells. Nonhomogeneous hypoautofluorescent regions in the transitional zone between centrally reduced AF and peripheral homogeneous AF showed increased cone spacing on AOSLO, consistent with cone loss (Fig. 3D). In regions of complete macular atrophy, AOSLO images showed bright oversaturated areas where cones were not seen, consistent with SD-OCT scans revealing extensive loss of outer retinal layers (Fig. 3F).

In some patients with extensive heterogeneous AF throughout the posterior pole, AOSLO images showed densely packed cones in contiguous mosaics interspersed with hyporeflective areas where few or no cones were seen (Figs. 2D, 2E). AOSLO images of these regions did not reveal well-defined changes in reflectivity or cone structure, suggesting more generalized degeneration of the RPE and the outer retina. Despite diffuse AF abnormalities, cone spacing abnormalities showed the same pattern seen in patients without extensive AF heterogeneity, with the most severe cone spacing abnormalities in the macula and more normal cone spacing near the ONH.

In addition, AOSLO images of STGD patients with central atrophy showed an annulus of decreased reflectance and sparse cones at the edge of the central atrophy. AOSLO images of F1P2 (Fig. 5), F3P1 (Fig. 1), F5P1 (Fig. 3), and F7P1 each show a parafoveal ring of decreased reflectivity corresponding to the edge of the scotoma in each patient. The AOSLO image in F1P1 (1 of 3 patients in the study who retained foveal fixation) showed a similar dim parafoveal ring in a region with progressive loss of visual function when imaged longitudinally. Over time, patient F1P1 showed progressively reduced foveal sensitivity, loss of cone reflectivity at the foveal center, expansion of the region of dim reflectance around the fovea, and evidence of intermittent use of an extrafoveal retinal locus for fixation (Fig. 7).

Lack of visible cones in dim regions of the AOSLO image may be attributed to poor image quality, scattering from media anterior to the photoreceptors, abnormal wave guiding properties in cones with abnormal outer segments or cones residing over abnormal RPE cells, or photoreceptor loss. The focal nature of the dim regions in which cones were not visualized

Diagram illustrates how measurements were taken. Distance was measured radially in degrees from the edge of the scleral rim. (**C**, **D**) Healthy subjects (*gray circles*); patients with STGD (*black triangles*).

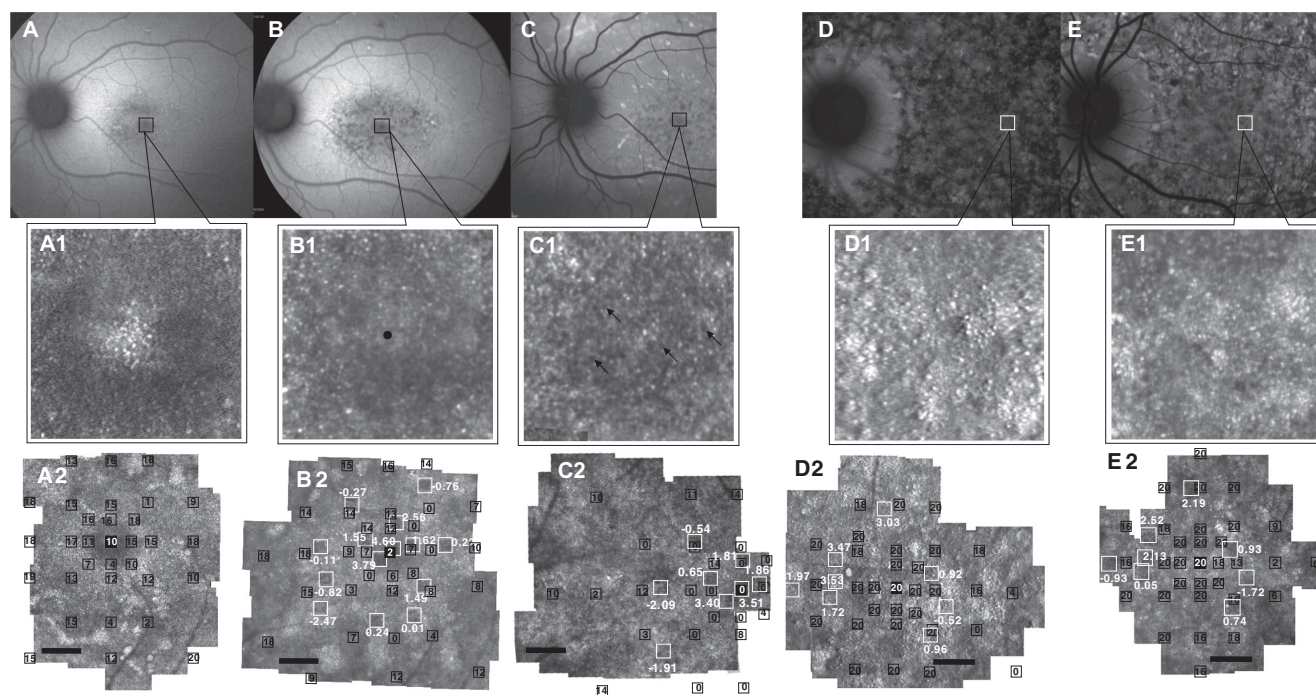


**FIGURE 7.** AF, AOSLO, and MP1 responses of F1P1 (A–C) and F2P1 (D, E) obtained over 27 months. F1P1: visit 1 (A), visit 2 (B) 15 months after visit 1, and visit 3 (C) 27 months after visit 1. The region of heterogeneous AF adjacent to the central region of reduced AF extended from the fovea in all directions. AOSLO images with MP1 sensitivities (*black boxes* and values, dB) and cone spacing measurements (*white boxes* and values, z-scores) show the disappearance of a foveal cone island followed by the appearance of scattered RPE cells (*arrows*; A1, B1, C1), coinciding with the loss of central visual sensitivity on microperimetry (A2, B2, C2). Fixation shifted superonasally at the 27-month visit; the vascular landmarks seen in the inferotemporal portions of (A2) and (B2) are not visualized. F2P1: visit 1 (D) and 2 (E) 27 months after visit 1. AOSLO images from both visits show coarse, disorganized cones at the fovea (D1, E1). Central visual sensitivity is preserved (D2, E2). Black scale bars, 1° (A2–E2).

makes poor image quality and scattering from media anterior to the photoreceptors less likely explanations. Elevations at the level of the RPE (Fig. 3E) or lipofuscin accumulation within RPE cells may affect properties of light reflected off the RPE cells and may prevent normal wave guiding through cone inner segments. Additionally, cones in the process of degeneration may lose their reflective properties but may retain visual function. In fact, the high dynamic range of SD-OCT often confirms the presence of IS/OS junctions, even though the cone mosaic is not directly visible with AOSLO. However, visualization of scattered RPE cells in the fovea of patient F1P1 (Fig. 7C1), in association with reduced visual acuity and visual sensitivity, suggests photoreceptors have been lost in at least some regions where cones are not visualized.

Recent studies<sup>31,70,74–76</sup> have correlated AF patterns with changes in visual function. In our study, dense central scotomas corresponded to reduced AF, consistent with atrophy of the RPE and overlying photoreceptors. Reduced visual sensitivity extended into regions with heterogeneous AF surrounding central RPE atrophy. Other studies have reported larger scotomas when centrally reduced AF was surrounded by regions of decreased AF rather than increased AF.<sup>70</sup> The observed relationship between scotoma size and AF abnormality suggests that abnormalities of lipofuscin deposition correlate with reduced visual function. In the present study, all patients with eccentric fixation used a PRL within regions in which a contiguous cone mosaic was present, although cone spacing was often abnormal. The PRL corresponded to a transitional zone between complete loss of the IS/OS junction layer in the central scotomas and preserved outer retinal layers distally, consistent with findings of a previous study.<sup>77</sup> The present study extends this observation with AOSLO images, showing that the PRL was located at the region closest to the anatomic fovea, where a contiguous cone mosaic was present (Figs. 1,

5). This observation suggests that a contiguous cone mosaic plays an important role in mediating visual acuity in patients with retinal degeneration.

A combination of imaging and functional modalities was used to monitor retinal changes over time in two patients with STGD. AOSLO images showed an increase in the width of a parafoveal ring of hyperreflective cones in F1P1, with concurrent degradation of cone mosaics centrally. The disappearance of visible foveal cones corresponded to a loss of central visual sensitivity and visual acuity and to intermittent use of extrafoveal fixation. The appearance of visible RPE cells in the progression of STGD, although our images give no information about the health of the remaining RPE cells. In F2P1, cone spacing remained abnormal over 27 months, in association with reduced sensitivity measured with microperimetry. In each of these patients, visual acuity remained stable despite evidence of progressive increases in cone spacing and reduced visual sensitivity, suggesting that visual acuity is an insensitive measure of cone loss and disease progression at the fovea in STGD. Although the small number of patients studied longitudinally is not adequate to predict how AOSLO cone spacing measures may change over time in other patients with STGD, our data suggest that in conjunction with measures of rod- and cone-mediated function,<sup>78</sup> measures of macular cone structure using AOSLO and SD-OCT may provide useful information about disease progression and response to experimental therapies as they are developed.

The longitudinal changes observed in this study support published models of STGD progression.<sup>11</sup> In patients with early disease, the accumulation of lipofuscin deposits in RPE cells produces focally increased AF and yellow flecks on fundus photography. Lipofuscin accumulation within RPE cells is followed by the death of overlying cones, leading to a decrease in

TABLE 2. Comparison of Clinical Measures with Stage of Disease Progression in Stargardt Patients

Modality	Stage I	Stage II	Stage III/IV	Stage V	Stage VI
Fundus photography	Normal	Yellow flecks	Yellow flecks	Focal regions of RPE atrophy	Atrophy
Fundus autofluorescence	Normal	Focally increased fundus autofluorescence	Mixed	Focally decreased fundus autofluorescence	Uniformly decreased fundus autofluorescence
AOSLO	Normal cone spacing	Irregular packing and increased cone spacing	Irregular packing and increased cone spacing; increased cone reflectance	Patchy cone loss with increased spacing, decreased cone reflectance	Oversaturated areas with no/few cones visible
Microperimetry	Normal sensitivity	Normal sensitivity	Mild sensitivity loss	Intermediate sensitivity loss	Severe sensitivity loss

photoreceptor density. With disease progression, excessive accumulation of lipofuscin leads to RPE atrophy, observed as decreased AF. In the present study, cone loss and abnormal wave guiding properties resulted in increased cone spacing and increased cone reflectance, followed by decreased visibility of cones in AOSLO images. In patients with advanced disease, uniformly decreased AF in combination with a loss of outer retinal structures on SD-OCT and a lack of visible cones on AOSLO indicate atrophy of RPE cells and photoreceptors. Although we did not perform measures of retinoid cycle slowing, we have compared our findings with the model of disease progression described by Cideciyan et al.<sup>11</sup> in STGD/ABCA4-related retinal degeneration (see Table 2).

Finally, the observation that AF is most normal in the annular region surrounding the optic nerve head in patients with STGD at all clinical stages corroborates previous study results,<sup>12,31,79</sup> although the parapapillary region may not be spared in up to 2% of patients.<sup>50</sup> In the present study, AF was most homogeneous in an annulus, at least 0.6 mm wide,<sup>12</sup> surrounding the optic disc in all patients, even those with extensive AF abnormality beyond the ONH (as in Fig. 2D). AOSLO images of the parapapillary region in STGD patients were nearly indistinguishable from normal, and cone spacing values were closest to normal at this location in all subjects. Several theories have been proposed to explain the phenomenon of parapapillary sparing, including lower rates of lipofuscin accumulation because of the decreased ratio of photoreceptor to RPE cells near the ONH, increased survival around the ONH caused by neurotrophic factors, and increased lipofuscin clearance near the ONH as a result of local changes in the choriocapillaris.<sup>12</sup> The results of the present study provide support for the observation that retinal and RPE structure is preserved in the parapapillary region in STGD patients and extend the observation beyond AF and visual function to include images of preserved cone structure.

## References

- Armstrong JD, Meyer D, Xu S, Elfervig JL. Long-term follow-up of Stargardt's disease and fundus flavimaculatus. *Ophthalmology*. 1998;105:448-457, discussion 457-448.
- Fishman GA, Farber M, Patel BS, Derlacki DJ. Visual acuity loss in patients with Stargardt's macular dystrophy. *Ophthalmology*. 1987;94:809-814.
- Glazer LC, Dryja TP. Understanding the etiology of Stargardt's disease. *Ophthalmol Clin North Am*. 2002;15:93-100, viii.
- Rotenstreich Y, Fishman GA, Anderson RJ. Visual acuity loss and clinical observations in a large series of patients with Stargardt disease. *Ophthalmology*. 2003;110:1151-1158.
- Birnbach CD, Jarvelainen M, Possin DE, Milam AH. Histopathology and immunocytochemistry of the neurosensory retina in fundus flavimaculatus. *Ophthalmology*. 1994;101:1211-1219.
- Eagle RC Jr, Lucier AC, Bernardino VB Jr, Yanoff M. Retinal pigment epithelial abnormalities in fundus flavimaculatus: a light and electron microscopic study. *Ophthalmology*. 1980;87:1189-1200.
- McDonnell PJ, Kivlin JD, Maumenee IH, Green WR. Fundus flavimaculatus without maculopathy: a clinicopathologic study. *Ophthalmology*. 1986;93:116-119.
- Steinmetz RL, Garner A, Maguire JI, Bird AC. Histopathology of incipient fundus flavimaculatus. *Ophthalmology*. 1991;98:953-956.
- Lopez PF, Maumenee IH, de la Cruz Z, Green WR. Autosomal-dominant fundus flavimaculatus: clinicopathologic correlation. *Ophthalmology*. 1990;97:798-809.
- Allikmets R. A photoreceptor cell-specific ATP-binding transporter gene (ABCR) is mutated in recessive Stargardt macular dystrophy. *Nat Genet*. 1997;17:122.
- Cideciyan AV, Aleman TS, Swider M, et al. Mutations in ABCA4 result in accumulation of lipofuscin before slowing of the retinoid cycle: a reappraisal of the human disease sequence. *Hum Mol Genet*. 2004;13:525-534.
- Cideciyan AV, Swider M, Aleman TS, et al. ABCA4-associated retinal degenerations spare structure and function of the human parapapillary retina. *Invest Ophthalmol Vis Sci*. 2005;46:4739-4746.
- Fishman GA, Stone EM, Grover S, Derlacki DJ, Haines HL, Hockey RR. Variation of clinical expression in patients with Stargardt dystrophy and sequence variations in the ABCR gene. *Arch Ophthalmol*. 1999;117:504-510.
- Gerth C, Andrassi-Darida M, Bock M, Preising MN, Weber BH, Lorenz B. Phenotypes of 16 Stargardt macular dystrophy/fundus flavimaculatus patients with known ABCA4 mutations and evaluation of genotype-phenotype correlation. *Graefes Arch Clin Exp Ophthalmol*. 2002;240:628-638.
- Molday LL, Rabin AR, Molday RS. ABCR expression in foveal cone photoreceptors and its role in Stargardt macular dystrophy. *Nat Genet*. 2000;25:257-258.
- Webster AR, Heon E, Lotery AJ, et al. An analysis of allelic variation in the ABCA4 gene. *Invest Ophthalmol Vis Sci*. 2001;42:1179-1189.
- Briggs CE, Rucinski D, Rosenfeld PJ, Hirose T, Berson EL, Dryja TP. Mutations in ABCR (ABCA4) in patients with Stargardt macular degeneration or cone-rod degeneration. *Invest Ophthalmol Vis Sci*. 2001;42:2229-2236.
- Azarian SM, Travis GH. The photoreceptor rim protein is an ABC transporter encoded by the gene for recessive Stargardt's disease (ABCR). *FEBS Lett*. 1997;409:247-252.
- Weng J, Mata NL, Azarian SM, Tzekov RT, Birch DG, Travis GH. Insights into the function of Rim protein in photoreceptors and etiology of Stargardt's disease from the phenotype in abcr knock-out mice. *Cell*. 1999;98:13-23.
- Sun H, Molday RS, Nathans J. Retinal stimulates ATP hydrolysis by purified and reconstituted ABCR, the photoreceptor-specific ATP-binding cassette transporter responsible for Stargardt disease. *J Biol Chem*. 1999;274:8269-8281.
- Mata NL, Tzekov RT, Liu X, Weng J, Birch DG, Travis GH. Delayed dark-adaptation and lipofuscin accumulation in abcr+/- mice:

- implications for involvement of ABCR in age-related macular degeneration. *Invest Ophthalmol Vis Sci.* 2001;42:1685-1690.
22. Mata NL, Weng J, Travis GH. Biosynthesis of a major lipofuscin fluorophore in mice and humans with ABCR-mediated retinal and macular degeneration. *Proc Natl Acad Sci U S A.* 2000;97:7154-7159.
  23. Cideciyan AV, Swider M, Aleman TS, et al. Reduced-illumination autofluorescence imaging in ABCA4-associated retinal degenerations. *J Opt Soc Am A Opt Image Sci Vis.* 2007;24:1457-1467.
  24. Delori FC, Dorey CK, Staurengli G, Arend O, Goger DG, Weiter JJ. In vivo fluorescence of the ocular fundus exhibits retinal pigment epithelium lipofuscin characteristics. *Invest Ophthalmol Vis Sci.* 1995;36:718-729.
  25. von Ruckmann A, Fitzke FW, Bird AC. Distribution of fundus autofluorescence with a scanning laser ophthalmoscope. *Br J Ophthalmol.* 1995;79:407-412.
  26. Delori FC, Fleckner MR, Goger DG, Weiter JJ, Dorey CK. Autofluorescence distribution associated with drusen in age-related macular degeneration. *Invest Ophthalmol Vis Sci.* 2000;41:496-504.
  27. von Ruckmann A, Fitzke FW, Bird AC. In vivo fundus autofluorescence in macular dystrophies. *Arch Ophthalmol.* 1997;115:609-615.
  28. Fish G, Grey R, Sehmi KS, Bird AC. The dark choroid in posterior retinal dystrophies. *Br J Ophthalmol.* 1981;65:359-363.
  29. Delori FC, Staurengli G, Arend O, Dorey CK, Goger DG, Weiter JJ. In vivo measurement of lipofuscin in Stargardt's disease: fundus flavimaculatus. *Invest Ophthalmol Vis Sci.* 1995;36:2327-2331.
  30. Hwang JC, Zernant J, Allikmets R, Barile GR, Chang S, Smith RT. Peripapillary atrophy in Stargardt disease. *Retina.* 2009;29:181-186.
  31. Lois N, Halfyard AS, Bird AC, Holder GE, Fitzke FW. Fundus autofluorescence in Stargardt macular dystrophy-fundus flavimaculatus. *Am J Ophthalmol.* 2004;138:55-63.
  32. Lois N, Halfyard AS, Bunce C, Bird AC, Fitzke FW. Reproducibility of fundus autofluorescence measurements obtained using a confocal scanning laser ophthalmoscope. *Br J Ophthalmol.* 1999;83:276-279.
  33. Lois N, Holder GE, Bunce C, Fitzke FW, Bird AC. Phenotypic subtypes of Stargardt macular dystrophy-fundus flavimaculatus. *Arch Ophthalmol.* 2001;119:359-369.
  34. Smith RT, Gomes NL, Barile G, Busuioc M, Lee N, Laine A. Lipofuscin and autofluorescence metrics in progressive Stargardt disease. *Invest Ophthalmol Vis Sci.* 2009;50:3907-3914.
  35. Sparrow JR, Nakanishi K, Parish CA. The lipofuscin fluorophore A2E mediates blue light-induced damage to retinal pigmented epithelial cells. *Invest Ophthalmol Vis Sci.* 2000;41:1981-1989.
  36. Schutt F, Davies S, Kopitz J, Holz FG, Boulton ME. Photodamage to human RPE cells by A2-E, a retinoid component of lipofuscin. *Invest Ophthalmol Vis Sci.* 2000;41:2303-2308.
  37. Boulton M, Dontsov A, Jarvis-Evans J, Ostrovsky M, Svistunenko D. Lipofuscin is a photoinducible free radical generator. *J Photochem Photobiol B.* 1993;19:201-204.
  38. Boulton M, McKechnie NM, Breda J, Bayly M, Marshall J. The formation of autofluorescent granules in cultured human RPE. *Invest Ophthalmol Vis Sci.* 1989;30:82-89.
  39. Holz FG, Schutt F, Kopitz J, et al. Inhibition of lysosomal degradative functions in RPE cells by a retinoid component of lipofuscin. *Invest Ophthalmol Vis Sci.* 1999;40:737-743.
  40. Dorey CK, Wu G, Ebenstein D, Garsd A, Weiter JJ. Cell loss in the aging retina: relationship to lipofuscin accumulation and macular degeneration. *Invest Ophthalmol Vis Sci.* 1989;30:1691-1699.
  41. Sparrow JR, Fishkin N, Zhou J, et al. A2E, a byproduct of the visual cycle. *Vision Res.* 2003;43:2983-2990.
  42. Ergun E, Hermann B, Wirtitsch M, et al. Assessment of central visual function in Stargardt's disease/fundus flavimaculatus with ultrahigh-resolution optical coherence tomography. *Invest Ophthalmol Vis Sci.* 2005;46:310-316.
  43. Gerth C, Zawadzki RJ, Choi SS, Keltner JL, Park SS, Werner JS. Visualization of lipofuscin accumulation in Stargardt macular dystrophy by high-resolution Fourier-domain optical coherence tomography. *Arch Ophthalmol.* 2007;125:575.
  44. Querques G, Leveziel N, Benhamou N, Voigt M, Soubrane G, Souied EH. Analysis of retinal flecks in fundus flavimaculatus using optical coherence tomography. *Br J Ophthalmol.* 2006;90:1157-1162.
  45. Querques G, Prato R, Iaculli C, et al. Correlation of visual function impairment and OCT findings in patients with Stargardt disease and fundus flavimaculatus. *Eur J Ophthalmol.* 2008;18:239-247.
  46. Voigt M, Querques G, Atmani K, et al. Analysis of retinal flecks in fundus flavimaculatus using high-definition spectral-domain optical coherence tomography. *Am J Ophthalmol.* 2010;150:330-337.
  47. Liang J, Williams DR. Aberrations and retinal image quality of the normal human eye. *J Opt Soc Am A Opt Image Sci Vis.* 1997;14:2873-2883.
  48. Liang J, Williams DR, Miller DT. Supernormal vision and high-resolution retinal imaging through adaptive optics. *J Opt Soc Am A Opt Image Sci Vis.* 1997;14:2884-2892.
  49. Roorda A, Williams DR. The arrangement of the three cone classes in the living human eye. *Nature.* 1999;397:520-522.
  50. Brainard DH, Roorda A, Yamauchi Y, et al. Functional consequences of the relative numbers of L and M cones. *J Opt Soc Am A Opt Image Sci Vis.* 2000;17:607-614.
  51. Roorda A, Metha AB, Lennie P, Williams DR. Packing arrangement of the three cone classes in primate retina. *Vision Res.* 2001;41:1291-1306.
  52. Roorda A, Williams DR. Optical fiber properties of individual human cones. *J Vision.* 2002;2:404-412.
  53. Pallikaris A, Williams DR, Hofer H. The reflectance of single cones in the living human eye. *Invest Ophthalmol Vis Sci.* 2003;44:4580-4592.
  54. Carroll J, Neitz M, Hofer H, Neitz J, Williams DR. Functional photoreceptor loss revealed with adaptive optics: an alternate cause of color blindness. *Proc Natl Acad Sci U S A.* 2004;101:8461-8466.
  55. Choi SS, Doble N, Hardy JL, et al. In vivo imaging of the photoreceptor mosaic in retinal dystrophies and correlations with visual function. *Invest Ophthalmol Vis Sci.* 2006;47:2080-2092.
  56. Wolfing JL, Chung M, Carroll J, Roorda A, Williams DR. High-resolution retinal imaging of cone-rod dystrophy. *Ophthalmology.* 2006;113:1019 e1011.
  57. Roorda A, Zhang Y, Duncan JL. High-resolution in vivo imaging of the RPE mosaic in eyes with retinal disease. *Invest Ophthalmol Vis Sci.* 2007;48:2297-2303.
  58. Duncan JL, Zhang Y, Gandhi J, et al. High-resolution imaging with adaptive optics in patients with inherited retinal degeneration. *Invest Ophthalmol Vis Sci.* 2007;48:3283-3291.
  59. Yoon MK, Roorda A, Zhang Y, et al. Adaptive optics scanning laser ophthalmoscopy images in a family with the mitochondrial DNA T8993C mutation. *Invest Ophthalmol Vis Sci.* 2009;50:1838-1847.
  60. Rha J, Dubis AM, Wagner-Schuman M, et al. Spectral domain optical coherence tomography and adaptive optics: imaging photoreceptor layer morphology to interpret preclinical phenotypes. *Adv Exp Med Biol.* 2010;664:309-316.
  61. Bowman KJ. A method for quantitative scoring of the Farnsworth Panel D-15. *Acta Ophthalmol (Copenh).* 1982;60:907-916.
  62. Lanthony P. [Evaluation of the desaturated Panel D-15, I: method of quantification and normal scores]. *J Fr Ophthalmol.* 1986;9:843-847.
  63. Spaide RF. Fundus autofluorescence and age-related macular degeneration. *Ophthalmology.* 2003;110:392-399.
  64. Marmor MF, Fulton AB, Holder GE, Miyake Y, Brigell M, Bach M. ISCEV standard for full-field clinical electroretinography (2008 update). *Doc Ophthalmol.* 2009;118:69-77.
  65. Rodieck RW. The density recovery profile: a method for the analysis of points in the plane applicable to retinal studies. *Vis Neurosci.* 1991;6:95-111.
  66. Sparrow JR, Parish CA, Hashimoto M, Nakanishi K. A2E, a lipofuscin fluorophore, in human retinal pigmented epithelial cells in culture. *Invest Ophthalmol Vis Sci.* 1999;40:2988-2995.
  67. Suter M, Reme C, Grimm C, et al. Age-related macular degeneration: the lipofuscin component N-retinyl-N-retinylidene ethanalamine detaches proapoptotic proteins from mitochondria and induces apoptosis in mammalian retinal pigment epithelial cells. *J Biol Chem.* 2000;275:39625-39630.

68. Boon CJ, Jeroen Klevering B, Keunen JE, Hoyng CB, Theelen T. Fundus autofluorescence imaging of retinal dystrophies. *Vision Res.* 2008;48:2569-2577.
69. Lois N, Holder GE, Fitzke FW, Plant C, Bird AC. Intrafamilial variation of phenotype in Stargardt macular dystrophy-Fundus flavimaculatus. *Invest Ophthalmol Vis Sci.* 1999;40:2668-2675.
70. Sunness JS, Steiner JN. Retinal function and loss of autofluorescence in Stargardt disease. *Retina.* 2008;28:794-800.
71. Wabbels B, Demmler A, Paunescu K, Wegscheider E, Preising MN, Lorenz B. Fundus autofluorescence in children and teenagers with hereditary retinal diseases. *Graefes Arch Clin Exp Ophthalmol.* 2006;244:36-45.
72. Lois N, Halfyard AS, Bird AC, Fitzke FW. Quantitative evaluation of fundus autofluorescence imaged "in vivo" in eyes with retinal disease. *Br J Ophthalmol.* 2000;84:741-745.
73. Schmitz-Valckenberg S, Fleckenstein M, Gobel AP, et al. Evaluation of autofluorescence imaging with the scanning laser ophthalmoscope and the fundus camera in age-related geographic atrophy. *Am J Ophthalmol.* 2008;146:183-192.
74. Popovic P, Jarc-Vidmar M, Hawlina M. Abnormal fundus autofluorescence in relation to retinal function in patients with retinitis pigmentosa. *Graefes Arch Clin Exp Ophthalmol.* 2005;243:1018-1027.
75. Preising MN, Wegscheider E, Friedburg C, Poloschek CM, Wabbels BK, Lorenz B. Fundus autofluorescence in carriers of choroideremia and correlation with electrophysiologic and psychophysical data. *Ophthalmology.* 2009;116:1201-1209 e1201-e1202.
76. Robson AG, Egan C, Holder GE, Bird AC, Fitzke FW. Comparing rod and cone function with fundus autofluorescence images in retinitis pigmentosa. *Adv Exp Med Biol.* 2003;533:41-47.
77. Gomes NL, Greenstein VC, Carlson JN, et al. A comparison of fundus autofluorescence and retinal structure in patients with Stargardt disease. *Invest Ophthalmol Vis Sci.* 2009;50:3953-3959.
78. Cideciyan AV, Swider M, Aleman TS, et al. ABCA4 disease progression and a proposed strategy for gene therapy. *Hum Mol Genet.* 2009;18:931-941.
79. Jayasundera T, Rhoades W, Branham K, Niziol LM, Musch DC, Heckenlively JR. Peripapillary dark choroid ring as a helpful diagnostic sign in advanced Stargardt disease. *Am J Ophthalmol.* 2010;149:656-660 e652.